# Design and Development of the Lifting and Propulsion Mechanism for a Biologically Inspired Water Runner Robot

Steven Floyd, *Student Member, IEEE*, and Metin Sitti, *Senior Member, IEEE*

***Abstract*—This paper describes the design and development of a novel robot, which attempts to emulate the basilisk lizard's ability to run on the surface of water. Previous studies of the lizards themselves have characterized their means of staying afloat. The design of a biomimetic robot utilizing similar principles is discussed, modeled, and prototyped. Functionally, the robot uses a pair of identical four bar mechanisms, with a 180° phase shift to achieve locomotion on the water's surface. Simulations for determining robot lift and power requirements are presented. Through simulation and experimentation, parameters are varied with the focus being a maximization of the ratio of lift to power. Four legged robots were more easily stabilized, and had a higher lift-to-power ratio than two legged robots. Decreases in characteristic length and running speed, and increases in foot diameter and foot penetration depth all cause a higher lift to power ratio. Experimental lift approached 80 gr, and experimental performance exceeded 12 gr/W for four legged robots with circular feet. This work opens the door for legged robots to become ambulatory over both land and water, and represents a first step toward robots which run on the water instead of floating or swimming.**

***Index Terms*—Aquatic propulsion, aquatic robot, biomimetic robots, lizard, locomotion, mobile robots, water running.**

## I. Introduction

SMALL, LIGHTWEIGHT animals have a large variety of flotation mechanisms available to them. There are spiders and insects that float using surface tension [1], [2], propel themselves using meniscus in the water [3], and secrete surfactants, utilizing marangoni flows to move. Larger animals have fewer options. Lizards, aquatic birds, and marine mammals, with their larger bulk and higher mass, utilize buoyancy, viscous drag, and momentum transfer [4].

Biomimetic robots are those machines that emulate some aspect of a living system. This paper describes the design and development of a robot that attempts to run on the surface of water in a manner similar to the basilisk lizard. Unlike other aquatic and amphibious robots that must swim or walk through the water [5]–[8], the water runner can stride upon it. This robot employs momentum transfer for both lift and propulsion, with negligible use of surface tension or buoyancy, which other water walking robots employ [2], [9], [10]. Hence, the robot will be the lightest of the amphibious robots, but the heaviest of the robots that locomote by water walking. The goal is not to copy nature, but to understand the principles of operation, and use this information to create novel machines to accomplish tasks, or to further increase understanding of the natural systems on which they are based.

The knowledge gained by this research will help expand the limits of legged robot locomotion. Possible studies include the development of bipedal or quadrupedal motion that can be utilized on both land and water. A legged robot capable of running on the water can use this technique to navigate semisubmerged environments without becoming bogged down or falling into sinkholes. Water walking could also be used as a short-range transition method for amphibious robots to change from land running to floating or swimming. This paper can also help increase the understanding of the basilisk lizard and its ability to walk on both land and water.

This paper first discusses how the basilisk lizard runs on water and the governing equations used for modeling in Section II. In Section III, a computer model of the water runner robot and its interactions with the water are examined in detail. In an attempt to determine optimum robot parameters, computer simulations are performed and validated by experimental results in Section IV. Using this information, a robot is fabricated and tested, with the results described in Section V.

## II. Basilisk Lizard Water Running

In order to emulate the water walking ability of basilisk lizards (*Basiliscus* sp.), this process must first be understood. There exist several papers on the lizard's shape and gait [14], [15], water running ability [12]–[15], foot shape [12], and foot-to-water interactions [4], [11]–[13], which mathematically characterize the forces and time scales, the results of which are summarized here.

The basilisk lizard is capable of running across the water's surface for several meters at approximately 1.5 m/s, or six body lengths per second, and a stepping rate of 5–10 Hz/leg. During the stepping cycle of each foot, there are three distinct phases that occur: the slap, stroke, and recovery phases [11]–[13]. Characterized by high impact forces over a short period of time, the slap phase occurs when the lizard's foot first impacts the water. Foot motion is primarily downward, and the magnitude of the

Manuscript received December 4, 2007; revised March 12, 2008. This paper was recommended for publication by Associate Editor H. R. Choi and Editor F. Park upon evaluation of the reviewers' comments.

The authors are with the NanoRobotics Laboratory, Department of Mechanical Engineering, Carnegie Mellon University, Pittsburgh, PA 15213 USA (e-mail: srfloyd@andrew.cmu.edu; sitti@cmu.edu).

Color versions of one or more of the figures in this paper are available online at http://ieeexplore.ieee.org.

Digital Object Identifier 10.1109/TRO.2008.924258

impulse force is a function of the foot's shape and velocity [12]:

$$I_{\text{slap}}^{\max} = \frac{4}{3}\rho r_{\text{eff}}^3 u_{\text{peak}} \tag{1}$$

where $I_{\text{slap}}^{\max}$ is the maximum slap impulse transferred to the foot, $r_{\text{eff}}$ is the empirically determined effective radius of the foot, and $u_{\text{peak}}$ is the peak velocity of the foot during the slap. The basis for this impulse force is developed in [11], and is based on the change of momentum of the fluid. For young, small, 2 gr lizards, the slap phase can provide more than 70% of the lift required to run on the surface of the water. As the lizards become larger, they primarily rely on the upward force provided by the stroke phase. Heavy lizards, 100 gr or more, use the slap phase for only 10%–20% of their total generated lift [12], [13].

The stroke phase begins just after the initial slap, when the lizard is dragging its foot through the water, pushing against it, and transferring momentum in the form of vortices [14]. Both lift and thrust are provided by this stroking motion, keeping the lizard aloft and propelling it forward. Drag on the foot is a combination of hydrostatic drag due to increasing depth, and inertial drag from momentum transferred to the fluid. The governing equation for the stroke phase is [11]:

$$D(t) = C_D^*[0.5S\rho u^2 + S\rho g h(t)] \tag{2}$$

where $D(t)$ is the time-varying drag force, $C_D^* \approx 0.703$ is the constant drag coefficient, $\rho$ is the density of water, $g$ is acceleration due to gravity, $S = \pi r_{\text{eff}}^2$ is the circular area over which drag is occurring, and $h(t)$ is the time varying depth of the foot.

Because of the high stepping speed, an air cavity is formed by the path the foot takes through the water during the slap and stroke phases. Afterward, in the recovery phase, the lizard must remove its foot from this cavity before it collapses. During the first part of the recovery, the basilisk lizard will curl the toes inward to prevent accidental drag on the cavity walls, and pull its foot upward, out of the cavity. For the remainder of the recovery, the step speed increases as the lizard propels its foot downward and prepares to slap the water surface in the next stride. No significant forces from the water are experienced by the lizard's foot during the recovery phase.

It is necessary for the lizard to slap, stroke, and retract its foot from the air cavity before it collapses, or it will sink. The time required for the cavity to collapse is nearly independent of the foot's velocity, and is purely a function of the foot's effective radius $r_{\text{eff}}$. From that collapse period, a minimum frequency $f_{\min}$ can be determined if one assumes that the lizard's leg spends about half the time in the water. The cavity-collapse time ($T_{\text{seal}}$) and minimum frequency were found for circular disks to be [12]:

$$T_{\text{seal}} = 2.285\sqrt{\frac{r_{\text{eff}}}{g}} \tag{3}$$

$$f_{\min} = \frac{1}{2T_{\text{seal}}}. \tag{4}$$

Four factors influence the lizard's ability to stay afloat: a) body mass; b) characteristic length; c) running speed; and d) shape of the foot. All of these variables are interrelated, and the morphological relations of these parameters to the lizard's water running have been characterized in [11]–[15].

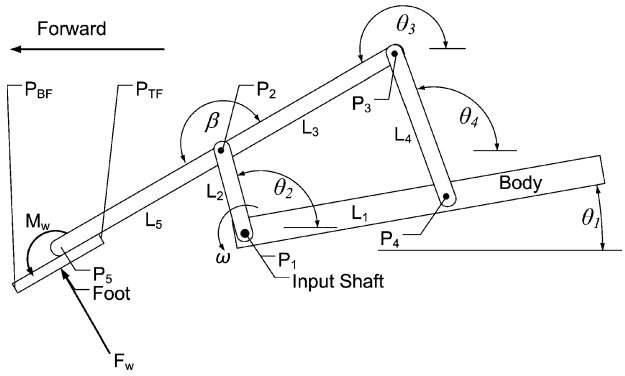


Fig. 1. Four bar mechanism used as legs in the water runner robot. Key points $P_2$ through $P_4$ are pin joints, while $P_1$ is driven by the motor. The foot is rigidly attached at $P_5$.

## III. Robot Modeling and Design

A simulation was created to model the robot behavior, examine forces and moments in the system, and determine the feasibility of creating a water running robot. As described in previous work [16], the water runner robot uses four bar mechanisms as legs. By using four bar mechanisms, the path traveled by the robot's foot through both air and water can be controlled. The links in a four bar mechanism are labeled in Fig. 1. Link $L_1$ is part of the body of the robot, and link $L_2$ is the input link, driven by the motor via the input shaft at point $P_1$. A foot of radius $R$ is rigidly attached at its center to the end of the output link $L_5$. The most distal and proximal points of the foot are $P_{\text{BF}}$ (bottom of the foot) and $P_{\text{TF}}$ (top of the foot), respectively. For each leg pair utilizing the same input shaft on opposite sides of the body, the input links are 180° out of phase, similar to the stepping mode of a basilisk lizard. When an additional pair of legs is added for a four-legged robot, the back input links lead the front input links on each side by 90°. This is done to present a more uniform load to the motor and to prevent unfavorable surface wave propagation. If the front legs lead the back legs, then the probability of the back legs stepping into the cavities formed by the front legs greatly increases.

In the simulation, the input link in each four bar mechanism is rotated at a constant angular velocity, $w$, and the forces from the legs are applied through frictionless pins to the robot's body. The body is free to move in a vertical direction, changing its distance from the surface of the water. The body is also free to pitch, but can neither roll nor yaw. For simplification, the water is assumed level and without waves, and it is further assumed that the cavities formed during the slap and stroke phases completely collapse before the next step is taken.

To provide a conservative estimate of the lift, only the stroke phase is used to determine lift in the computer model. The slap phase is disregarded because of its small effect on lift in 100 gr lizards, which can be as little as 10% of the total lift [12].

### A. Kinematics and Dynamics

Each leg on the water runner robot is a four bar mechanism; specifically, a Grashof linkage in the crank rocker configuration. Grashof linkages allow continuous relative motion of the shortest link and its adjacent links. The input link, link $L_2$ in Fig. 1, is the shortest link and rotates continuously. Also, the output link, link $L_4$ in Fig. 1, can move smoothly, and the path traced by the ankle, point $P_5$ in Fig. 1, is a smooth, continuous curve. The foot is rigidly attached to link $L_5$ at point $P_5$. For Grashof linkages, the links satisfy the constraints [17]:

$$s + l < p + q \tag{5}$$

where $s$ is the length of the shortest link, $l$ is the length of the longest link, and $p$ and $q$ are the lengths of the two remaining links. In non-Grashof linkages, which do not satisfy (5), continuous motion between any two links is not possible. Hence, a Grashof linkage was chosen because of the ease by which it can be driven by a motor.

By using trigonometry, employing complex notation, and noting that the pitch of the body is the angle $\theta_1$, one can determine each of the link angles labeled in Fig. 1. From these link angles, the location of key points $P_1$ through $P_5$, $P_{\mathrm{BF}}$, and $P_{\mathrm{TF}}$ relative to the origin can also be determined by successive application of positional relations, and noting that $P_1$ is initially at the origin [17].

Similar operations can be applied to additional pairs of legs. Key point positions are used to determine the penetration of the foot into the water and to keep track of the body position and orientation throughout the simulation. These are, in turn, used as failure criteria. For example, if the simulated body dips into the water or the body pitch becomes too great, that particular model is considered a failure.

Taking the first derivatives of the link angle formulas, the angular velocities of the links can be determined. The velocity of the center of the foot is used to determine which part of the step phase the robot is in: slap, stroke, or recovery. Similarly, the angular and linear accelerations are calculated. By averaging the accelerations of the correct key points, the linear acceleration of the center of mass of each link can be calculated. Using both the angular and linear accelerations, one can sum forces and moments for each link in the mechanism, thereby extracting the necessary reaction forces at the pins, and the required torque applied to the input link.

### B. Forces Exerted by the Water

During the recovery phase, it is assumed that there is no interaction between the foot and the water, and all forces and moments within a leg are a result of link accelerations. The stroke phase is defined within the simulation as the period of time when some part of the foot is below the water line and the velocity of the ankle ($V_5$) is downward and toward the rear of the robot. Forces exerted during the stroke phase act solely upon the robot's foot, not on any submerged portion of the leg. Further, all shear forces on the foot are assumed negligibly small by comparison to normal forces.

The computer model incorporates a distributed foot that can be partially submerged depending on its position. The percent of submersion, $p$, is found via

$$p = \frac{y_{\mathrm{water}} - y_{\mathrm{BF}}}{y_{\mathrm{TF}} - y_{\mathrm{BF}}} \tag{6}$$

where $y_{\mathrm{water}}$ is the height of the water, $y_{\mathrm{BF}}$ is the height of the bottom of the foot, and $y_{\mathrm{TF}}$ is the height of the top of the foot. If the foot is totally submerged, i.e., $y_{\mathrm{water}} \geq y_{\mathrm{TF}}$, then $p$ is set to 1.

The effect of the water on the foot is determined via an integral over the length of the submerged section. As there is both linear and angular velocity, the velocity distribution over the area of the foot must be taken into account. If one assumes that rigid components are used, then the velocity distribution along the bottom of the foot will have to be linear, and can be found from the velocity of two points:

$$\vec{\mathbf{v}}(s) = \frac{\vec{v_{\mathrm{TF}}} - \vec{v_{\mathrm{BF}}}}{2R} s + \frac{\vec{v_{\mathrm{TF}}} + \vec{v_{\mathrm{BF}}}}{2} \tag{7}$$

where $s$ is a variable representing a point along the bottom of the foot from $P_{\mathrm{BF}}$ to $P_{\mathrm{TF}}$, $v(s)$ is the velocity at point $s$, $v_{\mathrm{TF}}$ and $v_{\mathrm{BF}}$ are the velocities of the top and bottom of the foot, respectively, and $R$ is the radius of the foot.

Once this distribution in velocity is known, an integral of (2) can be performed over the bottom of the foot to find the total lift force:

$$a(s) = \vec{\mathbf{v}}(s) \cdot \vec{\mathbf{n}} \tag{8}$$

$$h(s) = (y_{\mathrm{water}} - y_{\mathrm{BF}}) \left(1 - \frac{s+R}{2pR}\right) \tag{9}$$

$$F_w = C_D^* \rho \int_{-R}^{-R+2pR} (\sqrt{R^2 - s^2})(2gh(s) + a(s)|a(s)|) ds \tag{10}$$

$$M_w = C_D^* \rho \int_{-R}^{-R+2pR} (\sqrt{R^2 - s^2})(2gh(s) + a(s)|a(s)|)(-s) ds \tag{11}$$

where $a(s)$ is the component of the velocity normal to the foot at $s$ and $s$ is taken along the length of the foot from $P_{\mathrm{BF}}$, the most submerged point of the foot to the water level. $\vec{\mathbf{v}}(s) \in \mathbb{R}^3$ is the velocity vector at $s$, $\vec{\mathbf{n}} \in \mathbb{R}^3$ is a vector normal to the foot, and $h(s)$ is the depth of point $s$. $F_w$ and $M_w$ are the total force and moment the water exerts on the foot, respectively. These forces are applied on the foot, as in Fig. 1.

By adjusting the integrand in (10), the effects of noncircular feet can be simulated if it is assumed the coefficient of drag does not change significantly for different foot geometries. (This assumption is later found to be false.)

### C. Link Lengths

The set of four bar mechanisms that satisfy the Grashof criterion (5) is infinite. While the set of *realizable* link lengths is significantly smaller, it too is infinite. For any given set of link lengths, the trajectory followed by the foot is unique, and

TABLE I
OPTIMIZED LINK LENGTHS DETERMINED IN SIMULATION

| Link Lengths (mm) | $L_1$ | $L_3$ | $L_4$ | $L_5$ |
|---|---|---|---|---|
| Length Ranges for the Optimized Top 10% of Simulated Designs | 55 - 68 | 60 - 85 | 45 - 55 | 50 - 65 |
| Mean ± 1 Standard Deviation of the Above Values | 63 - 67 | 75 - 83 | 45-46 | 53 - 63 |

the lift provided by the legs, the power consumed to move the legs through space and water, and the steady-state separation between the body and the water will be functions of that trajectory. To determine preferable link lengths, a fitness criteria must be used to evaluate each simulated design. Increased mass that the linkages can lift is, of course, positive aspect, whereas the increased power used is negative effect. For practical operation, some clearance between the bottom of the robot and the surface of the water is desired, so that too must be encouraged in optimization steps. Analogous to a cost function, the fitness of each design can be evaluated by:

$$\frac{M}{P_{\text{ave}}}\left[A\frac{\bar{y}-y_{\text{water}}}{L_2}+B\right] \tag{12}$$

where $M$ is the mass that the robot can lift, $P_{\text{ave}}$ is the average power consumed to lift that weight, and $\bar{y}$ is the average height of the robot above the water, all determined in simulation. Any set of link lengths that could not lift 30 gr/pair of legs and maintain an average height of at least 26.5 mm above the water was assigned a fitness value of 0. $A$ and $B$ are weights used in the fitness equation with $A = 0.4$ and $B = 0.6$. This metric and these values were chosen based on experience with the water running robot, and not on any rigorous analysis of performance or stability. More systematically chosen weights or a different fitness equation may be utilized in future. In addition to the average power used to evaluate the fitness of each design, peak power was also examined as a useful metric when determining the requirements of any motor for experimental prototypes. This measure of fitness is solely concerned with the robot's ability to generate lift and stay above the water, and changes in forward thrust do not affect the fitness of a particular design.

Employing this measure of fitness, optimization using both a gradient descent and simple multidimensional search was performed. An arbitrary Grashof linkage was generated, then varied until a local maximum was reached, or the Grashof criterion (5) was no longer satisfied. The procedure was then restarted with a different set of link lengths. The range of link lengths that had had fitness within the top 10% are presented in Table I, where $L_2$ was held constant at 21.8 mm.

Throughout the optimization process, points $P_1$ and $P_4$ (as labeled in Fig. 1) are kept horizontal relative to the body, $\beta$ is kept at $180^\circ$, and the foot is kept parallel to link $L_5$. These assumptions were made to facilitate easy fabrication of models for testing, and do not necessarily represent the optimal designs choices.

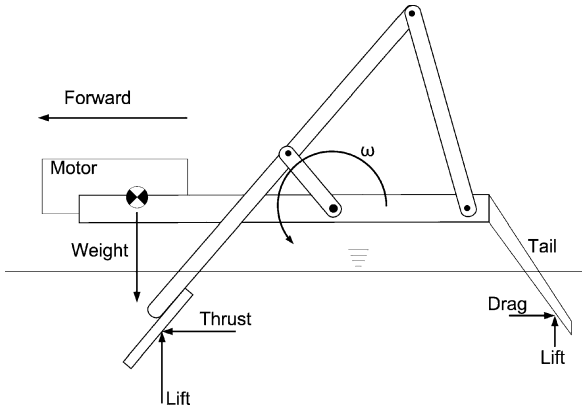


Fig. 2. Forces generated by a pair of legs and two methods to stabilize a two-legged water runner. The magnitude of the moment and the effectiveness of each method is dependent upon the specific link lengths used.

### D. Force Balance

The chief concerns of a free water running system are total lifting ability and dynamic stability. Averaged over time, the total lift of the system must equal the weight of the robot. Unlike quadrupedal walking on land, where the weight is distributed over two or three legs (depending on the gait), when water running, only one leg is producing the majority of the lift at a given time. Each leg must, therefore, provide a peak lift force greater than the body weight. Through simulations, the peak lift force per leg was found to be approximately 120% of the robot's weight. This excess lift is in good agreement with the forces produced by the lizard [14].

### E. Moment Balance

When considering dynamic stability, the ability of the robot to return to steady state while running, one must be concerned with both the pitch and the roll of the robot. Yaw of the robot affects the steering, not the ability to stay afloat, so it is not addressed at this time.

By exerting both an upward lift and a forward thrust while maintaining the body above the water, a net moment is created by each leg with a tendency to drive the rear of the robot into the water. As shown in Fig. 2, both the lift and the thrust contribute to this moment, and the severity of the problem is dependent on the exact four bar link lengths utilized. For a two legged robot, one way to counteract this moment is to shift the center of mass an appropriate distance in front of the drive axle in an attempt to cancel out the generated moment. Another option that can be used alone or in conjunction with the center of mass placement is to utilize a tail that can generate drag and perhaps lift, if it displaces enough water. Both of these stabilization methods are shown in Fig. 2. The basilisk lizard employs both of these methods to stay upright while running on water, and can actively adjust its posture to change its center of mass and the drag and lift provided by its tail.

For four-legged systems, the undesired moment due to thrust is doubled. At any given time, the forces experienced by the body include gravity, lift, and thrust at each pin, generated by each

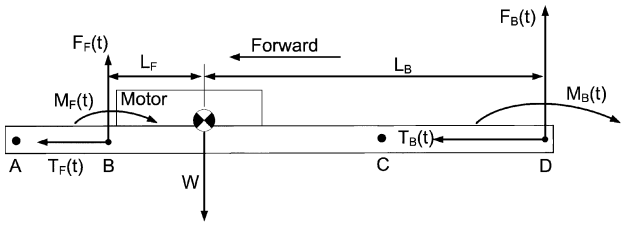


Fig. 3. Lumped forces and methods of stabilizing a four-legged water runner. By using different link lengths for the front and back pairs of legs, the lift and moment generated by each will be different.

of the four bar mechanisms. These forces can be represented by net lifts, thrusts, and couples for the front and back pairs of legs. In Fig. 3, $F_F(t)$ and $T_F(t)$ are the sums of the lift and thrust forces at pins A and B at time $t$, $M_F(t)$ is the net moment due to lift forces at A and B, taken at pin B, and $L_F$ is the distance between the center of mass and pin B. Similarly, $F_B(t)$ and $T_B(t)$ are the sums of the lift and thrust forces at pins C and D at time $t$, $M_B(t)$ is the net moment due to lift forces at C and D, taken at pin D, and $L_B$ is the distance between the center of mass and pin D.

Like the two-legged robots, four-legged water runners can utilize a tail and/or the placement of the center of mass to decrease the magnitude of the undesired moment. In addition, one can use different link lengths for the front and back pairs of legs, making $F_B$ greater than $F_F$ on average, which increases the restoring moment about the center of mass. This effect can be further amplified by making $L_B$ much larger than $L_F$. If one assumes that the water runner is relatively level, one can determine the sum of moments about the center of mass:

$$\sum M(t) = -F_F(t)L_F + F_B(t)L_B - M_F(t) - M_B(t) \quad (13)$$

$$F_F(t) = F_A(t) + F_B(t), \qquad F_B = F_C(t) + F_D(t) \quad (14)$$

$$M_F(t) = F_A(t)L_{1,F}, \qquad M_B(t) = F_C(t)L_{1,B} \quad (15)$$

where $M(t)$ is the moment at time $t$, $F_A$ through $F_D$ are the lift forces at the pins, $L_{1,F}$ is the length between pins A and B, and $L_{1,B}$ is the length between pins C and D. Ideally, one would want the sum of moments to be exactly zero at all time, but that is not possible in this dynamic system. What is achievable though is a time-averaged moment equal to zero. Assuming the time-averaged moment is zero, one can determine the effectiveness of each of the moment-compensation techniques in a four-legged water runner.

*1) Center Length:* By increasing $L_B$ relative to $L_F$, the lift required from the front and back pairs of legs varies greatly. One can, therefore, transition from an unrealizable robot—which requires negative lift on the front pair of legs to stay relatively level—to a stable system where both pairs of legs contribute to the overall lift of the system. This transition is shown for a representative four bar linkage in Fig. 4. All values are nondimensional to demonstrate general results, which are true for all sets of link lengths. From examination, it is apparent that too short a water runner will be unable to remain stably level, and will tilt until it sinks. As the length increases, $F_F$ increases while $F_B$ decreases. While the two values do not need to be

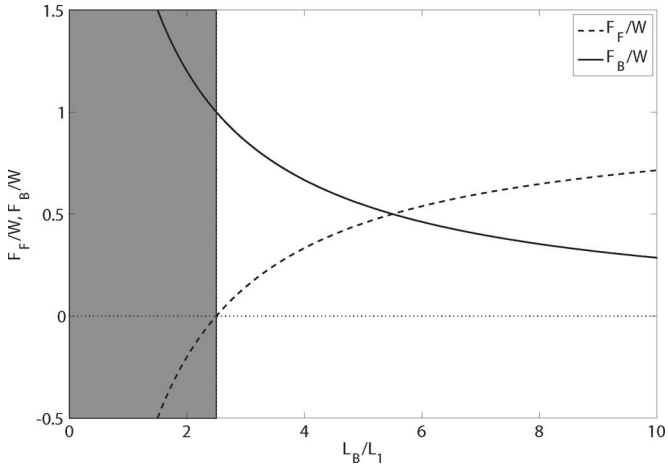


Fig. 4. Simulation of the required lift from front and back pair of legs as percentage of weight $W$ due to increases in $L_B/L_1$ at $L_F/L_1 = 0.5$. Designs that require negative lift for the front pair of legs (gray area) are nonrealizable.

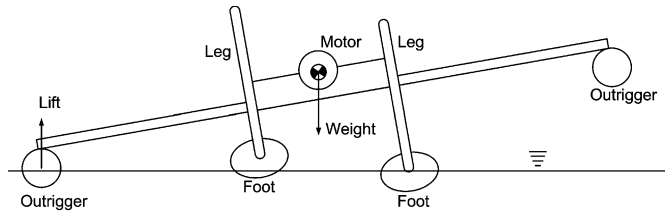


Fig. 5. Water runner robot as seen from the front. Any rolling can be corrected by using buoyant outriggers that generate lift when the roll angle causes them to be submerged.

equal, inequality implies that the robot will not run levelly, or that selective scaling must also be employed.

*2) Selective Scaling:* A second method to ensure moment balance is to utilize different link lengths for the front and back legs. Because link lengths exist that have much higher performance as compared to others, as found earlier, it seems illogical to employ anything except a high-performance set of link lengths. One can then change the length scaling (LS) between front and back, thereby employing high-performance link lengths, but generating different amounts of lift. One can also run the front and back sets of legs at different speeds, by using gearing or an additional motor. The advantages and disadvantages of each of these choices will be discussed in Section IV. In either case, by utilizing selective scaling, one can set the lengths $L_F$ and $L_B$ to a reasonable, realizable value, but one does not need to ensure that $F_F = F_B = W/2$.

As for the possibility of the robot rolling, this can be stabilized if there exists a restoring force, which increases with increasing depth of the feet on one side of the robot. Section IV will address this and show that as the feet penetrate deeper, they generate more lift. But, it should be noted that this increase in lift can be mitigated by changes in attack angle due to the roll angle of the robot. A solution, as shown in Fig. 5 is to use buoyant outriggers that generate lift when submerged. By placing the outriggers far from the center of mass, a large moment is generated when the roll angle changes and an outrigger submerges.

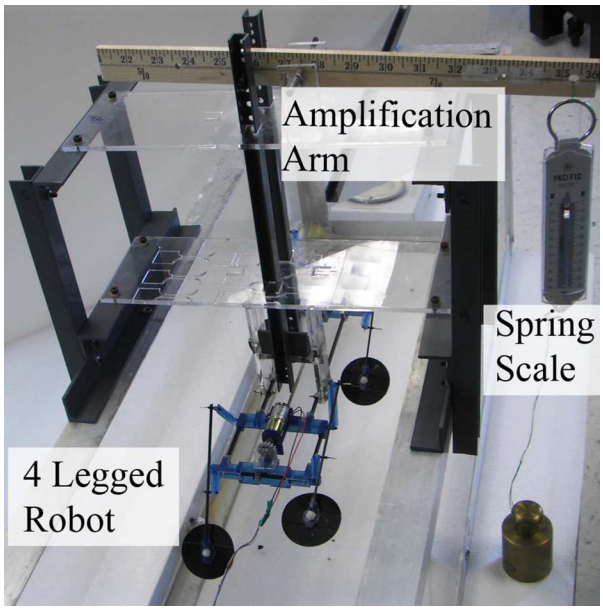


Fig. 6. Photograph of the test rig used to determine lift in each of the experiments.

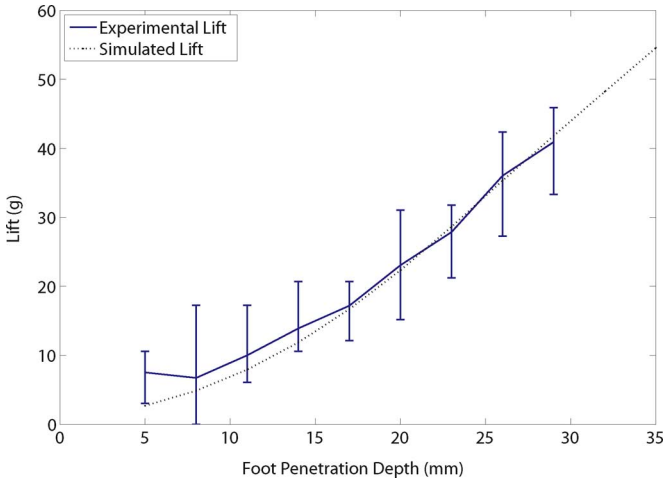


Fig. 7. Simulated and experimental data of change in lift force with respect to change in depth for a four-legged robot. Foot diameter is 40 mm, and running speed is 6.0 Hz.

## IV. Model Validation

It is critical to experimentally validate much of the work done solely by simulation in previous work [16]. To do so, a test rig that allows measurement of the lift generated by a water runner robot was constructed, and several critical robot parameters were varied. Presented here is simulated behavior along with experimental data to demonstrate the accuracy of the computer model, and validate its use for the purposes of extrapolation, and generating inferences in cases where experimentation is excessively time consuming, difficult, costly, or impossible due to technological limitations.

Experiments were performed using the testing setup shown in Fig. 6. The robot is free to move in a vertical direction, but all other motions are suppressed. It is held aloft by the amplification arm, which is, in turn, connected to a spring scale. Spring displacement is scaled down by a factor of 4:1 to the robot, keeping it at a relatively constant height above the water. When running on water, the robot generates lift, which decreases the amount the spring scale is stretched. This lift is also scaled down by a factor of 4:1 from the robot to the spring. Spring displacement at rest and while the robot is running is measured.

Calibration is performed by pulling upward on the amplification arm at the location where the robot is pinned by using a 100 gr weight and a pulley. The water level is varied to determine the lift at a given separation between the water and the axle of the drive shaft. This separation can, in turn, be related to a depth that the foot penetrates the water, with a value of zero when the foot just touches the water at the lowest point in its trajectory. Because of this, most measurements, both in simulation and experiment, are found as a function of foot penetration depth.

To determine whether a change in the model leads to an improvement, a generic variable called *performance* was defined as the ratio of the lift force in grams to the power required in watts. Higher performance is, therefore, preferable because a robot with a finite energy source (such as a battery or capacitor) will get the most lift for whatever power it is capable of investing. Performance is used instead of fitness, as defined in (12), so that the effect of changing the distance between the robot and the water could more clearly be understood.

The four bar mechanism used in these experiments has link lengths $L_1 = 65.0$ mm, $L_2 = 21.8$ mm, $L_3 = 74.8$ mm, $L_4 = 45.4$ mm, and $L_5 = 54.4$ mm. These link lengths were determined using the optimization method described in Section III.

### A. Foot Penetration Depth

In order to run on water with any chance of stability, there must be a restoring force whenever deviations from operating conditions, such as the steady-state height above the water or steady-state pitch angle, occur. Most notably, there must be an increase in lift if the robot sinks, and a decrease of lift if the robot rises. If this restoring force is linear with position, then the time-averaged leg interactions with the water are similar to spring forces. The "stiffer" this spring, whether or not it is linear, the more easily the robot can stay at a constant height.

Fig. 7 displays the spring-like interaction with the water. As the penetration of the foot into the water increases, i.e., as the depth increases, lift increases. Note that the computer model is accurate when predicting the average lift.

### B. Power Requirements

For any miniature mobile robot, the power requirement is a crucial metric, as the power supply is always limited [18]. While capable of predicting lift with accuracy, the computer model cannot *a priori* predict power requirements. To do this, one must first make measurements of the motor and the system they intend to use to determine efficiency and frictional losses. The simulation only reports the required power acted upon the

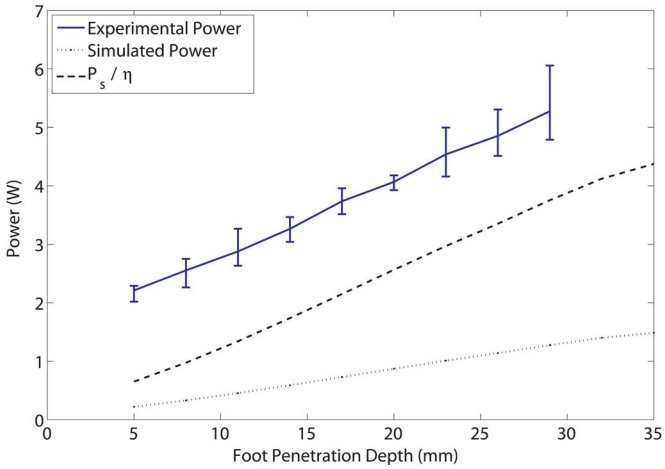


Fig. 8. Simulated power, experimental power, and simulated power divided by measured efficiency, for different foot penetration depth. The difference between the experimental power and $P_s/\eta$ is the frictional power loss ($F_f$) in the system. Foot diameter is 40 mm and running speed is 6.0 Hz.

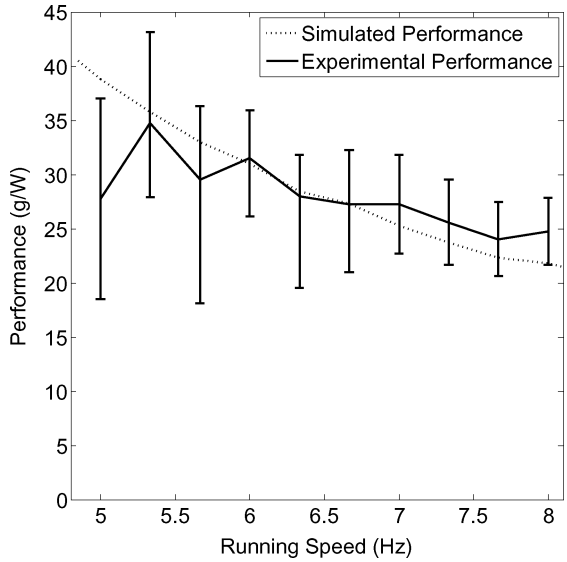


Fig. 9. Simulated and experimental effects of changing the running speed of the robot. Both were performed for a robot with 40 mm diameter feet, at a foot penetration depth of 26 mm. The minimum required frequency, $f_{\min}$, for these feet is 4.85 Hz from (4).

water to stay afloat. As a postprocessing step, the simulated power can be used to determine a theoretical input power by simply using the measured efficiency and frictional losses of the system. For the lift data presented in Fig. 7, the experimental and simulated power data are presented in Fig. 8. The equation to derive the power requirements from the simulated power is as follows:

$$P_i = \frac{1}{\eta} P_s + F_f \tag{16}$$

where $P_i$ is the necessary input power, $\eta$ is the efficiency of the entire motor, gearbox, and robot system, $P_s$ is the simulated peak required power, and $F_f$ is the measured frictional loss. To ensure the regularity of all measurements of performance (defined as the ratio of lift in grams to the peak power in watts), the simulated power will be used. This way, if motors with higher efficiency or systems with lower friction are employed, the lift and power requirements can be determined from simulation data, instead of reperforming an experiment.

### C. Running Speed

Any reasonable, attainable frequency can be used, provided the robot stays above the cavity collapse frequency, $f_{\min}$ from (4). Basilisk lizards run at frequencies ranging from 5 to 10 Hz, but few exceed 10 Hz. It may be that muscles are incapable of such speeds without doing irreparable damage to joints or bones. Motors are limited only by the strength of the gearbox and their torque capabilities. By performing these tests, we can establish whether high- or low-speed robots will have a higher probability of success. Results are shown in Fig. 9.

Drag force on the foot is dependent on the square of the foot's velocity (2). Velocity is dependent on both the rotational speed of the input link, and on the lengths of the links. Hence, higher speeds and larger characteristic lengths would correspond to greater lifts. But, the power required to produce those speeds is dependent on the product of the moment and the velocity.

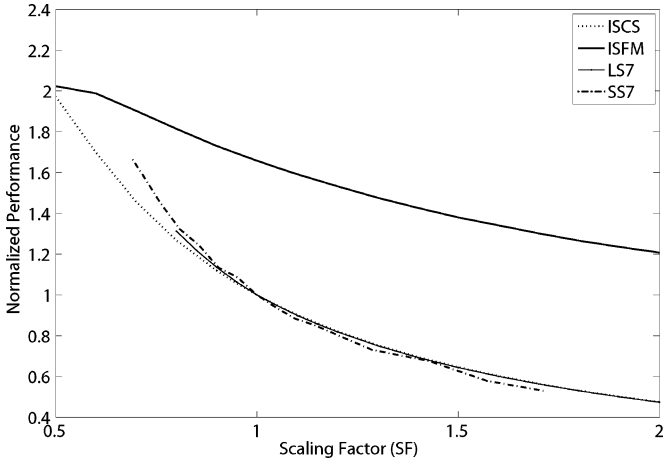


Fig. 10. Simulated effect on normalized performance due to changes in the scale factor. ISCS: isometric scaling of link lengths and foot diameter at a constant speed of 7 Hz; ISFM: isometric scaling of link lengths and foot diameter at $f_{\min}$; LS: length scaling of link lengths at a constant speed of 7 Hz and foot diameter of 40 mm; SS: speed scaling at constant link lengths with foot diameter of 40 mm.

$$D(t) \propto u^2 \propto \omega_2^2 L_{\text{char}}^2 \tag{17}$$

$$P = \omega_2 T \propto \omega_2 (D(t) L_{\text{char}}) = \omega_2^3 L_{\text{char}}^3 \tag{18}$$

where $\omega_2$ is the angular velocity of link 2, $L_{\text{char}}$ is the characteristic length of the links, and $T$ is the torque the motor must apply to maintain the constant rotation of link 2. Total power has a cubic dependence on characteristic length and speed, while lift, which is proportional to drag, has only a square dependence on those parameters. These results demonstrate that a slower, smaller robot is the preferable design, as seen in Fig. 10. The low experimental performance at very low running frequencies

in Fig. 9 is likely due to occasional cavity collapses, a hazard when operating so near the cavity collapse frequency.

### D. Scaling Effects

To corroborate the scaling derivation presented earlier and visualize the effect of increasing characteristic length and/or speed, a graph of normalized performance is presented in Fig. 10. Four different methods of scaling are simulated in this figure. Isometric scaling at a constant speed (ISCS) is found by scaling all of the link lengths, and the foot diameter, by a constant scaling factor (SF). The running speed is held constant at 7 Hz. Isometric scaling at $f_{\min}$ (ISFM) is simulated by scaling all of the link lengths and the foot diameter by SF, but also decreasing the running speed to the minimum frequency at that foot diameter, found by the application of (4). LS is found by scaling all of the link lengths by SF, but maintaining a constant foot diameter of 40 mm, and a constant running speed of 7 Hz. Lastly, speed scaling (SS), as previously discussed, is simulated by scaling the running speed relative to 7 Hz while maintaining constant link lengths and a constant foot diameter of 40 mm. For each of these simulations, the performance was normalized to their respective performances at $\mathrm{SF} = 1$.

For the ISCS, LS, and SS cases, performance scaling is so similar that the three lines are nearly identical. All three of these scaling methods conform to approximately $1/\mathrm{SF}$, because each linearly scales either $L_{\mathrm{char}}$ (ISCS and LS) or $\omega_2$ (SS). ISFM conforms to $1/\sqrt{\mathrm{SF}}$ because of the dual effects of $L_{\mathrm{char}}$ scaling linearly, and $\omega_2 = f_{\min}$ scaling with $1/\sqrt{\mathrm{SF}}$ (4). These exercises confirm the initial conclusion that a slower and smaller robot is the preferable design, but they further add that if increases in size are necessary, they should be isometric, and the speed should be maintained at or near $f_{\min}$.

### E. Foot Shape

*1) Elliptical Feet:* While (2) was developed for vertical entry of circular cross sections entering the water, other shapes might provide better lift for an investiture of power. To wit, the lizard feet are not circular; they are more like elongated hands [12]. Hence, experiments were run with elliptical feet in two orientations with the long axis: 1) parallel and 2) perpendicular to the centerline of the body. Both the circular and elliptical feet are connected to the ankle at the center of the major and minor axes, and all had the same area. The performances of these ellipses are shown in Fig. 11. In the simulation, both orientations of elliptical feet and circular feet with the same area have the same performance. Comparing these results with those in Fig. 7, where circular feet experimentally provide lift almost equal to simulation, one notes a marked decrease in performance when using elliptical feet in either orientation. Both sets of experimental data are strictly below the performance in simulation. Of especially low performance are the elliptical feet perpendicular to the body axis, which seem to have decreased performance when closer to the water. The most likely reason elliptical feet have decreased performance as compared to circular feet is that the coefficient of drag used in (2) is not the same for noncircular cross-sectioned feet, thereby rendering the assumption used to generate the simulated performance incorrect.

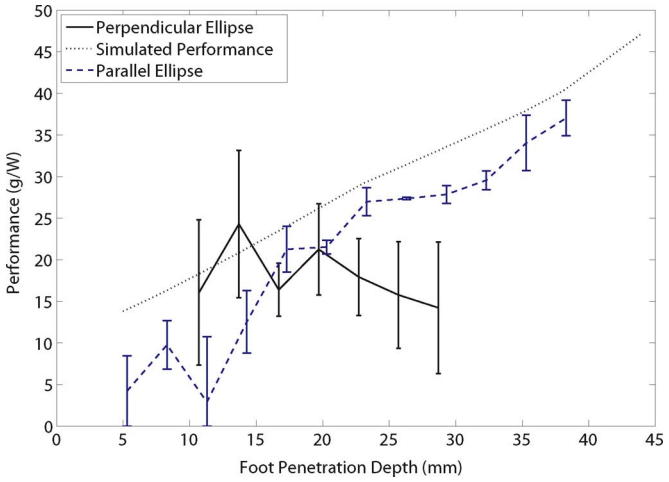


Fig. 11. Simulated and experimental effect of employing elliptical feet. Tests were run at 6 Hz. Major axis length was 50 mm and minor axis length was 30 mm. Simulated performance for both ellipse orientation and for circular feet with the same area are all very similar, and are represented by the simulated performance line. Experimental error bars shifted horizontally slightly to facilitate viewing.

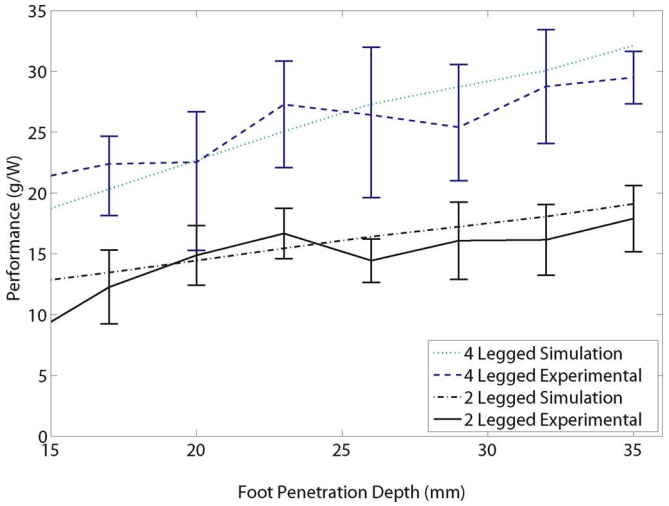


Fig. 12. Simulated and experimental effect of changing the diameter of the robot's circular feet. If done at a constant speed, there is only a small increase in performance. If the frequency is reduced to $f_{\min}$, there is a linear increase in performance. Experimental error bars shifted horizontally slightly to facilitate viewing.

*2) Diameter:* Lift force and power are both proportional to the area of the foot; so, one may assume that an increase in foot diameter would lead to little or no gain in performance. As seen in Fig. 12, this is only true when the foot diameter is increased at constant speed. But, from (4), an increase in foot diameter corresponds to a decrease in $f_{\min}$. Hence, the robot is capable of water running at a lower speed. It was determined earlier that robots that run more slowly have better performance at a constant foot diameter; so, it is no surprise that there is a marked increase in performance if the foot diameter is increased and the speed is dropped to near $f_{\min}$.

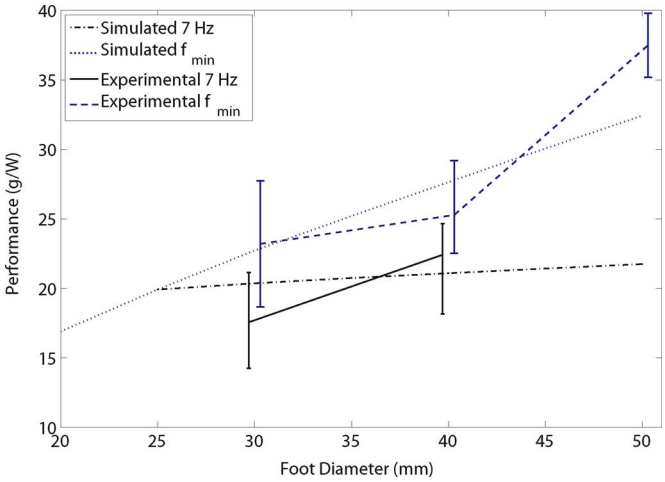


Fig. 13. Simulated and experimental effects of adding additional legs to the robot. Running speed was 6.66 Hz for 40 mm diameter circular feet.

From this, we can conclude that the small, slow robot should have large feet for its size. The actual maximum size of the foot will be constrained by the robot geometry and the ability of the motor to produce torque.

### F. Two Versus Four Legs

By increasing the number of legs, the net lift force required from each stroke event is halved, but the number of stroke events is doubled. By shifting the secondary set of legs by 90° relative to the first pair, the load on the motor is made more constant, and is not substantially increased. The additional legs provide essentially double the lift, but only create a marginal increase in motor torque. So, by adding an additional pair of legs, there is a increase in performance of approximately 20%–80%, depending on foot penetration depth, with higher depths corresponding to greater increases in performance. These changes in performance are displayed in Fig. 13.

## V. Robot Fabrication and Experiments

Two water runner robots were constructed; one high-strength robot for model validation used in Section IV and one low-weight runner, which was tested on open water. The primary structural components for both robots are made of a copolymer material composed of triethylene glycol dimethacrylate ester (45%–55%), urethane acrylate resin (35%–45%), and polypropylene glycol monomethacrylate (1%–5%). Utilizing a 3-D systems invision HR 3-D printer, this material is printed in the desired shape, and was used to make the motor support structure, sections of the robot body, and the input links ($L_2$) in the four bar mechanisms. Pultruded carbon fiber bars are used for structural strengthening, support, and the remaining links in the four bar mechanism legs. Gears and drive shaft are made of acrylonitrile butadiene styrene (ABS). Feet were fabricated on a GCC Venus Laser using polyoxymethylene homopolymer (Delrin). Initial testing and computer model verification was done on the test rig shown in Fig. 6 using a single HG-16 (Copal) gearmotor at gearings 30:1, 50:1, or 60:1 with power supplied by an Agilent E3610A dc power supply. Frequency of operation was determined using an Extech Instruments Digital StroboTach stroboscope tachometer. All pin joints are 1-mm diameter steel pins.

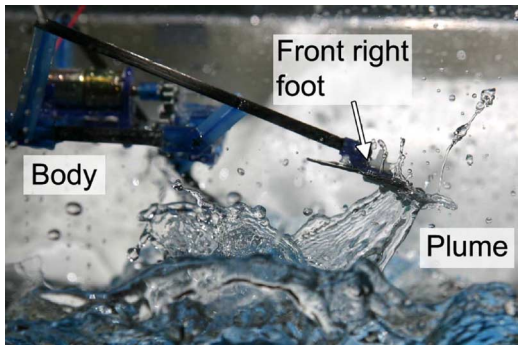


Fig. 14. Side-view photograph of the water plume dragged from the cavity by the foot during the recovery phase of the robot's step.

The experimental efficiency of the motors ranged from 30% to 50%, with frictional and air losses between 0.9 and 1.5 W for two-legged robots and between 1.3 and 1.7 W for four-legged robots. Using this information along with (16), experimental power usage was in agreement with the simulation power. Experimental performance in terms of simulated power, i.e., assuming 100% efficiency and no frictional losses, exceeded 50 gr/W. Performance in terms of real input power exceeded 12 gr/W, which is substantially lower than the simulated work, due primarily to the low efficiency of the motors used and the high friction in the system.

### A. Plume Formation

When observing the water runner robot utilizing a high-speed camera (3000 ft/s), we observed the formation of plumes of water dragged from the cavity to the edge of the foot during foot retraction [19]. This plume can be seen in one frame of the footage, shown in Fig. 14. The plume results in excess splashing, additional drag on the foot, and may cause cavity deformation or collapse. At the very least, it represents an unnecessary expenditure of energy.

To combat the formation of this plume, feet with folding edges were implemented. Basilisk lizards close their feet during the recovery phase of their steps in the water, so nature may have already dealt with this problem. That being said, the basilisks still splash as they run, so the problem may be unsolvable. The feet were cut along lines spaced 5 mm from the center of a 40 mm diameter foot. These removed sections were then reconnected to the main part of the foot via a layer of tape on the bottom, as shown in Fig. 15. Feet were connected to the legs via ankles, which acted as physical stops, preventing the feet from folding backward during each down stroke. Taken together, these features would allow the "toes" to fold downward when the foot was being retracted from the air cavity, but remain flat throughout the slap and stroke phase. It was found

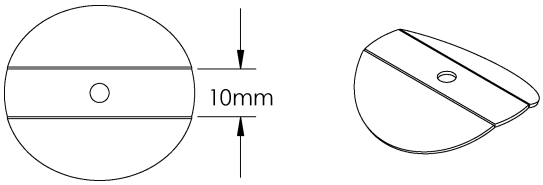


Fig. 15. Sketch of the compliant feet used on the water runner robot.

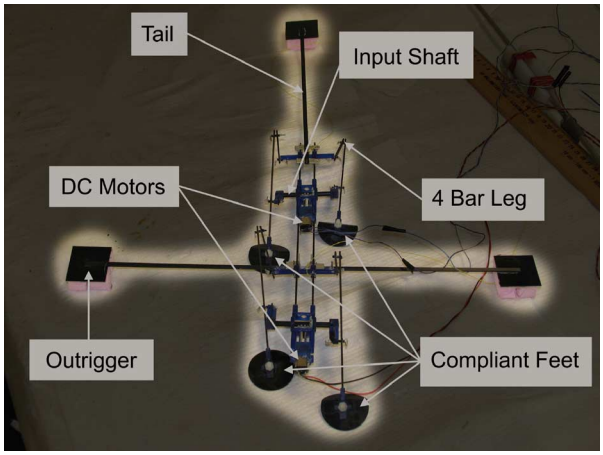


Fig. 16. Photograph of the water runner constructed using information gained from testing and computer simulations, as seen from the top.

empirically that front/back cut lines were more effective at decreasing plume formation and increasing lift than left/right cut lines. This directional compliance decreased the incidence of plume formation, and caused a marked increase in lift, bringing experimental results very close to computer predictions. These compliant feet were used on the water runner shown in Fig. 16.

### B. Open Water Testing

Using the results gleaned in Section IV, the optimization performed in Section III-C, the two moment compensation techniques and the outriggers discussed in Section III-E, and the compliant feet described in Section V-A, a water runner robot was constructed, and is shown in Fig. 16. This water runner robot was constructed with two Sanyo NA 50:1 gearmotors, one for the front pair of legs and one for the back pair. Power was supplied by lithium polymer batteries. The outriggers and the tail were composed of four cubes of expanded polystyrene (Styrofoam) each approximately 20 mm on a side, providing a lift of approximately 4.6 gr when completely submerged. These cubes were connected to 40 mm Delrin squares, which were attached to the body through pultruded carbon fiber bars. In this way, the lift provided by the outriggers and tail could be varied between 4.6 and 18.6 gr each. The center of each outrigger was located 20 cm out from the center of mass and the center of the tail was located 40 cm behind the center of mass.

Running on open water has been achieved with both off and on board power. Videos can be found online at [19]. With an on board power supply weighing 22 gr, total robot weight was 103 gr, including outriggers (approximately 9 gr) and tail (approximately 6 gr). For this robot, the tail provided 18.6 gr of lift when fully submerged. The lift provided by each outrigger was varied between 4.6 and 18.6 gr when fully submerged. Assuming that the tail was fully submerged, and each outrigger was half submerged, the robot provided between 65.8 and 79.8 gr of lift. With only one buoyant cube on each side of the robot, any lift provided by the outriggers is equal to or less than the total weight of the outriggers.

Running speed varied inversely to the lift provided by the robot, and ranged between 80.6 and 49.9 cm/s, though no exact relationship between running speed and lift has yet been determined. It is likely that any future design that does not include either outriggers or a tail would have a faster running speed due to decreased drag. Power consumption was not explicitly monitored when running on the open water, but has been found to be approximately 6.3 W when the robot is subjected to similar conditions in a more controlled environment. Taking the mean lift of 72.8 gr, and using the controlled power expenditure, this leads to a performance of 11.6 gr/W, similar to the performance of the high strength water runner used in model validation. Both of these speeds are much slower than the basilisk lizard's 1.5 m/s.

Four photos of the water runner robot running on water without outriggers are shown in Fig. 17. In the first frame, the right front leg is at the top of its path, the compliant foot is flat, and the robot is relatively horizontal. At the lowest point of its trajectory, the foot is stroking through the water in the second frame, creating a cavity and providing lift to the water runner. Somewhat obscured by the water cavity, the compliant foot has collapsed in the third frame and is pulling out of the water. In the fourth frame, the right foot is completely out of the water, has pulled a less energetic plume than can be seen in Fig. 14, and the robot has rolled onto its left side due to the lack of outriggers. The emphasis line is dashed in the final frame because the link $L_5$ is partially obscured by the foot.

## VI. Discussion

The current system has low power efficiency, only 30%–50%, because of the choice of motors and the high frictional losses. Over 1.5 W of power is currently lost to friction at 6 Hz running speed, mostly due to the rubbing of unlubricated parts on each other. Basilisk lizards expend an estimated 0.033 W/gr of weight to run on water [11], a performance of 30 gr/W, but current prototypes require 0.083 W/gr, or performance of 12 gr/W, making them much less power efficient. An autonomous robot would need to be lighter and more energy efficient with greater degrees of freedom. Even at low efficiency and high losses, power requirements are well within the capabilities of lithium polymer batteries, which provide high current at very low weight.

A tail that provides both lift and drag is used on the current robot to stabilize rotation in the pitch direction, for the reasons

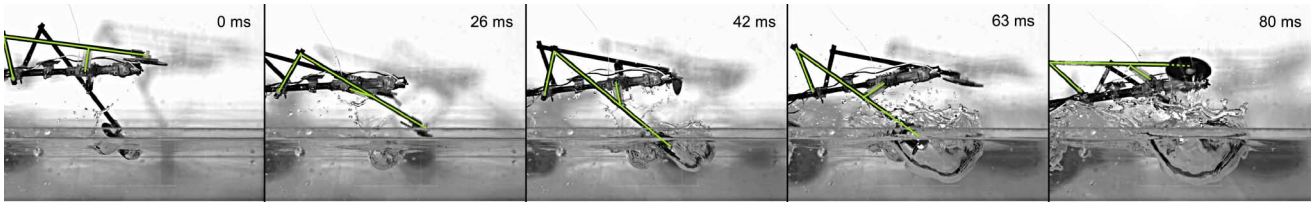


Fig. 17. High-speed footage of the water runner in a small aquarium. Links $L_2$ through $L_5$ on the right front leg have been highlighted for emphasis. Time in milliseconds is provided in the top right corner of each frame.

mentioned in Section III-E. Without such a tail, the robot rotates toward its rear, completely submerging the back set of legs, and changing the dynamics sufficiently to cause it to sink. In order to remove the need for such a tail, both design methods discussed in Section III-E, controlling the center length, and selective scaling of the back pair of legs, are being investigated.

Buoyant outriggers are used on the current robot because it is unstable in the roll direction. Criteria for stability in the roll direction, including the effect of the roll moment of inertia, the running frequency, and the forces and moments generated by the water when the robot is not perfectly horizontal, are being investigated. A water running robot that requires no buoyant forces for stabilization is the direction of our future work.

In addition, control systems and steering mechanisms are currently being investigated. Also, being analyzed and tested are devices with additional degrees of freedom, including, but not limited to, actuated ankles, individual leg speed control, and energy storing springs for land locomotion. Of great interest for amphibious locomotion is the possibility of including additional joints to make each four bar mechanism dynamic, allowing adjustment of the ankle trajectory. The ultimate goal is a fully autonomous and amphibious water runner capable of traversing both land and water.

## VII. Conclusion

In this paper, a robot that mimics the water running ability of the basilisk lizard is simulated, analyzed, and developed. A predictive computer model is developed and validated through experimental confirmation. Parameters are varied in simulation and experiment to increase the performance of both the two and four-legged robots. The separation between the front and back pairs of legs in a four-legged robot is a critical design criterion to establish stable water running, while two-legged robots are much more difficult to stabilize. It was found that increases in both characteristic length and speed decrease the robot performance, while increases in foot diameter and a higher foot penetration depth increase performance. Elliptical feet were found to have lower performance than circular feet in experiments. Experimental performance in terms of input power exceeded 12 gr/W for four-legged robots with circular feet. Future work will be toward autonomous water and land running using high-efficiency and high-power-density actuators and low-weight batteries.

## Acknowledgment

The authors would like to thank J. Palmisano for his early designs, testing, and experimental methods, T. Keegan and K. Oner for fabricating and testings multiple prototypes and devising better measurement techniques, L. Weiss for the use of the high-speed camera, and the NanoRobotics Laboratory members for their support and suggestions.

## References

[1] R. Suter, O. Rosenberg, S. Loeb, and H. Long, "Locomotion on the water surface: Propulsive mechanisms of the Fisher Spider *Dolomedes Triton*," *J. Exp. Biol.*, vol. 200, pp. 2523–2538, Oct. 1997.

[2] D. Hu, B. Chan, and J. Bush, "The hydrodynamics of water strider locomotion," *Nature*, vol. 424, pp. 663–666, Aug. 2003.

[3] D. Hu and J. Bush, "Meniscus-climbing Insects," *Nature*, vol. 437, pp. 733–736, Sep. 2005.

[4] J. Bush and D. Hu, "Walking on water: Biolocomotion at the interface," *Annu. Rev. Fluid Mech.*, vol. 38, pp. 339–369, Jan. 2006.

[5] A. Boxerbaum, P. Werk, D. Quinn, and R. Vaidyanathan, "Design of an autonomous amphibious robot for surf zone operation," in *Proc. IEEE/ASME Int. Conf. Adv. Intell. Mechatron.*, Jul. 2005, pp. 1459–1464.

[6] A. Crespi, A. Badertscher, A. Guignard, and A. Ijspeert, "AmphiBot I: An amphibious snake-like robot," *Robot. Auton. Syst.*, vol. 50, pp. 163–175, Mar. 2005.

[7] S. Guo, T. Fukuda, and K. Asaka, "A new type of fish-like underwater microrobot," *IEEE/ASME Trans. Mechatronics*, vol. 8, no. 1, pp. 136–141, Mar. 2003.

[8] C. Georgiadis, A. German, A. Hogue, H. Liu, C. Prahacs, A. Ripsman, R. Sim, L. Torres, P. Zhang, M. Buehler, G. Dudek, M. Jenkin, and E. Milios, "AQUA: An aquatic walking robot," in *Proc. IEEEE/RSJ Int. Conf. Intell. Robots Syst.*, Sep. 2004, pp. 3525–3531.

[9] Y. S. Song and M. Sitti, "Surface tension driven biologically inspired water strider robots: Theory and experiments," *IEEE Trans. Robot.*, vol. 23, no. 3, pp. 578–589, Jun. 2007.

[10] H. Takonobu, K. Kodaira, and H. Takeda, "Water Striders muscle arrangement-based robot," in *Proc. IEEE/RSJ Int. Conf. Intell. Robots Syst.*, Aug. 2005, pp. 1754–1759.

[11] J. Glasheen and T. McMahon, "Vertical water entry of disks at low Froude number," *Phys. Fluids*, vol. 8, pp. 2078–2083, Aug. 1996.

[12] J. Glasheen and T. McMahon, "Size-dependence of water-running ability in Basilisk lizards (*Basiliscus Basiliscus*)," *J. Exp. Biol.*, vol. 199, pp. 2611–2618, Dec. 1996.

[13] J. Glasheen and T. McMahon, "A hydrodynamic model of locomotion in the Basilisk Lizard," *Nature*, vol. 380, pp. 340–342, Mar. 1996.

[14] T. Hsieh and G. Lauder, "Running on water: Three-dimensional force generation by basilisk lizards," *PNAS USA*, vol. 101, pp. 16784–16788, Nov. 2004.

[15] S. Hsieh, "Three-dimensional hind limb kinematics of water running in the plumed basilisk lizard (*Basiliscus plumifrons*)," *J. Exp. Biol.*, vol. 206, pp. 4363–4377, Dec. 2003.

[16] S. Floyd, T. Keegan, J. Palmisano, and M. Sitti, "A novel water running robot inspired by Basilisk Lizards," in *Proc. IEEE/RSJ Int. Conf. Intell. Robots Syst.*, Oct. 2006, pp. 5430–5436.

[17] [Online]. Available: http://iel.ucdavis.edu/chhtml/toolkit/mechanism

[18] M. Sitti, "Microscale and nanoscale robotics systems (grand challenges of robotics)," *IEEE Robot. Autom. Mag.*, vol. 14, no. 1, pp. 53–60, Mar. 2007.

[19] [Online]. Available: http://nanolab.me.cmu.edu/projects/waterrunner/

**Steven Floyd** (S'04) received the B.S. degree in mechanical engineering (*summa cum laude*) from Washington University in St. Louis, St. Louis, MO, in 2005. He is currently working toward the M.S. and Ph.D. degrees in mechanical engineering at the Department of Mechanical Engineering, Carnegie Mellon University, Pittsburgh, PA.

His current research interests include design and control of biologically inspired robotics, design and fabrication of microelectromechanical systems, microscale manipulation and assembly, microrobotics, analog electronics design, and magnetic power transfer and actuation.

Mr. Floyd received the National Science Foundation Graduate Research Fellowship (2005) and the second prize in the World RoboCup Nanogram Demonstration League (2007).

**Metin Sitti** (S'94–M'00–SM'08) received the B.Sc. and M.Sc. degrees in electrical and electronic engineering from Bogazici University, Istanbul, Turkey, in 1992 and 1994, respectively, and the Ph.D. degree in electrical engineering from the University of Tokyo, Tokyo, Japan, in 1999.

During 1994–1996, he was with the CAD/CAM Robotics Department, TUBITAK Marmara Research Center, Kocaeli, Turkey, as a Research Engineer. During 1999–2002, he was a Research Scientist and a Lecturer in the Department of Electrical Engineering and Computer Sciences, University of California, Berkeley. During 2007, he was the Adamson Career Faculty Fellow at Carnegie Mellon University (CMU), Pittsburgh, PA, where he is currently an Associate Professor in the Mechanical Engineering Department and the Robotics Institute. His current research interests include miniature mobile robots, biologically inspired micro/nanosystems, and micro/nanoscale manipulation and manufacturing systems.

Dr. Sitti was the recipient of the National Science Foundation CAREER Award and the CMU Struminger Award in 2005, the second prize in the World RoboCup Nanogram Demonstration League in 2007, the Best Biomimetics Paper Award in the IEEE Robotics and Biomimetics Conference in 2004, the Best Paper Award in the IEEE/RSJ International Conference on Intelligent Robots and Systems in 1998, and the Best Video Award in 2002 in the IEEE Robotics and Automation Conference. He was the Distinguished Lecturer of the IEEE Robotics and Automation Soceity for 2006–2008. He is the Vice-President of the Technical Activities in the IEEE Nanotechnology Council, and he is the Co-Editor-in-Chief of *Journal of Micro/Nano-Mechatronics*.